Quantitative Imaging: Physics integrated and machine learning based models in MRI

Michael Hintermüller[1,2]

Mathematical Colloquium @ Chinese University of Hong Kong

[1]Weierstrass Institute; [2]Humboldt University of Berlin

Online talk, December 3, 2021

Content

1. Preliminary on (quantitative) MRI
2. Mathematical understanding of MRF-based methods
3. Integrated physics-based method for qMRI
4. Using learning-informed physical models
   4.1 Some analytical aspects
   4.2 Application to qMRI

Preliminary on (quantitative) MRI

Magnetic resonance imaging

Three major steps in the current routine of MRI experiment:

- Aligning magnetic nuclear spins in an applied constant magnetic field B_0
- Perturbing this alignment via radio frequency (RF) pulse B_1
- Applying magnetic gradient field G to distinguish individual contributions

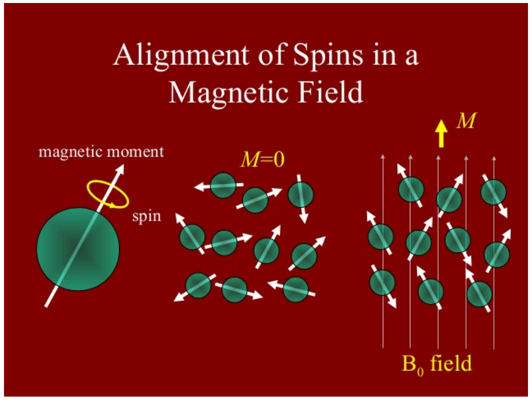

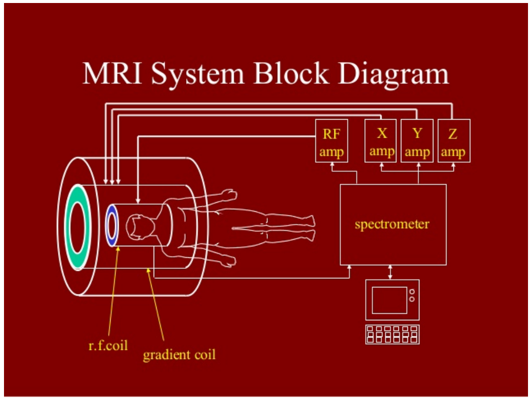

Abbildung: MRI diagram (Published in Health and Medicine)

Magnetic resonance imaging

„All models are wrong, but some are useful“

George Box, 1976

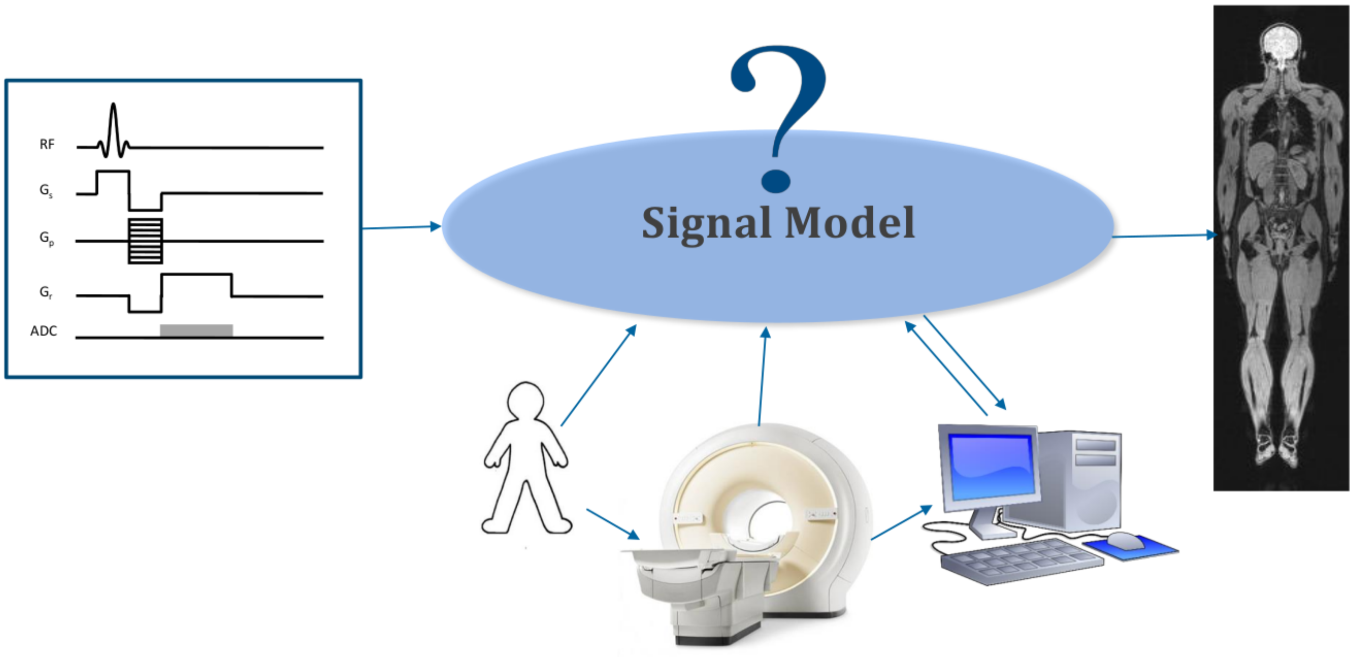

Abbildung: Courtesy of Dr. Mariya Doneva (Philips)

Bloch equations and simulation of MRI data

- Bloch equations (physical law behind the nuclear magnetic resonance):

$$\frac{\partial m(\mathbf{x},t)}{\partial t} = \gamma m(\mathbf{x},t) \times B(\mathbf{x},t) - \left(\frac{m_x(\mathbf{x},t)}{T_2}, \frac{m_y(\mathbf{x},t)}{T_2}, \frac{m_z(\mathbf{x},t)-1}{T_1} \right)^\top .$$

  γ is a known parameter, $B = B_0 + B_1 + (0,0,G\cdot\mathbf{x})$. T_1 and T_2 are longitude and transverse relaxation times, respectively, tissue (space) dependent.
- Some phrases in MRI:
  - Flip angles α: Characterized by the RF pulses B_1 field $\alpha(t) = \gamma \int_0^t |B_1(s)|ds$.
  - Repetition time TR: The length of the time period from one pulse to the next pulse.
- Selecting a slice at $z = z_0$

$$Y =: P\mathcal{F}(\rho T_{xy} m(\cdot,\cdot,z_0)).$$

  P denotes a subsampling operator, $T_{xy}m := m_x + i m_y$, and ρ is proton density.

This is an idealized mathematical description, e.g., coil sensitivity are ignored.

Subsampling patterns

Cartesian subsampling pattern

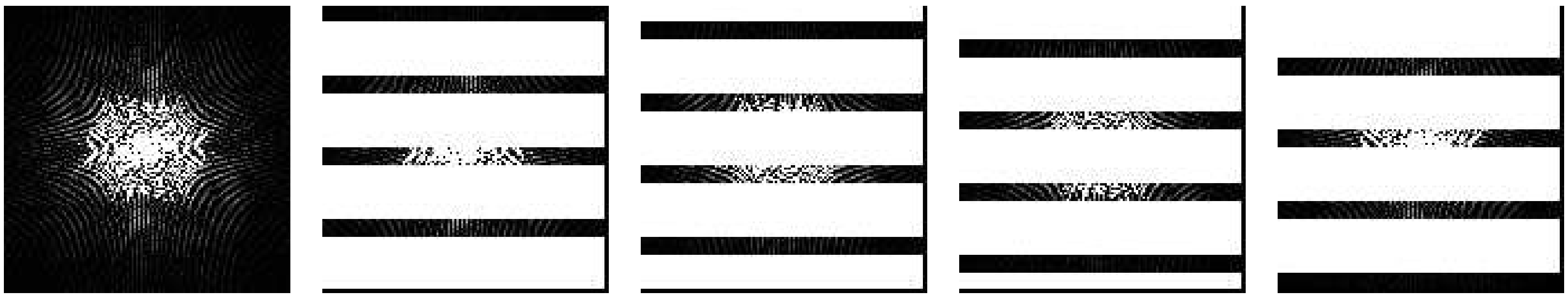

Radial subsampling pattern

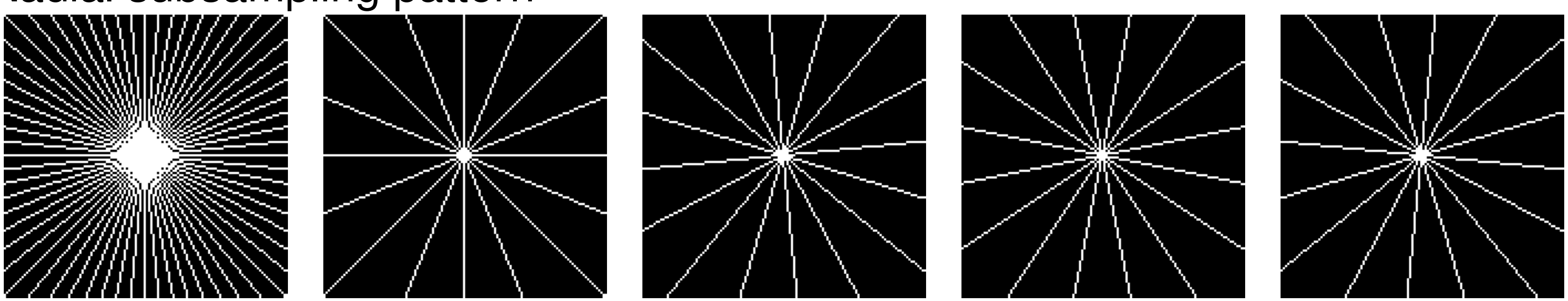

Qualitative MRI v.s. Quantitative MRI

Example of K-space data

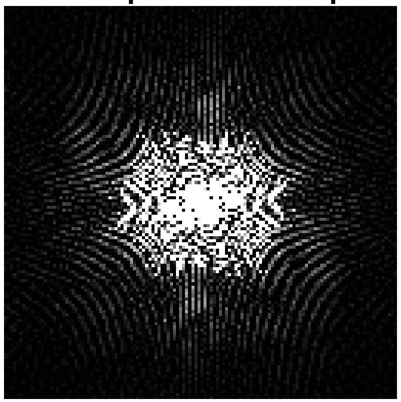

from under-sampled data

Example of qualitative MRI

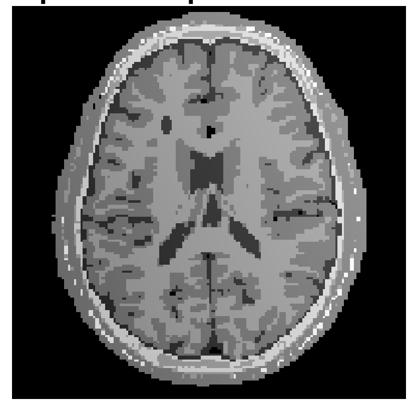

Example of quantitative MRI parameters (T_1, T_2, ρ)

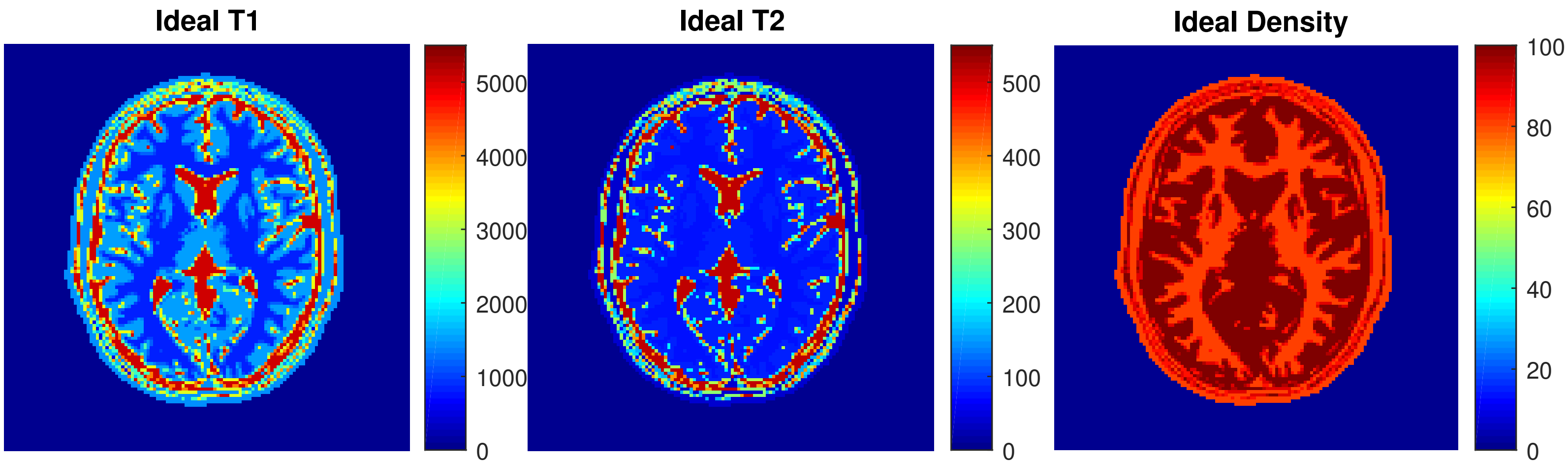

Qualitative MRI v.s. Quantitative MRI

Example of K-space data

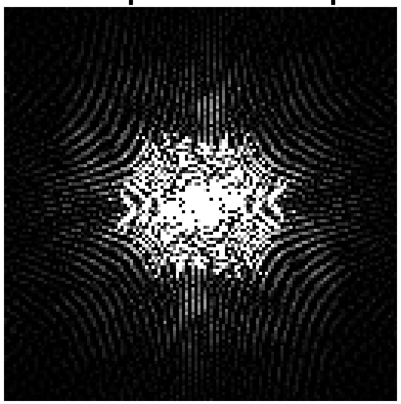

from under-sampled data

Example of qualitative MRI

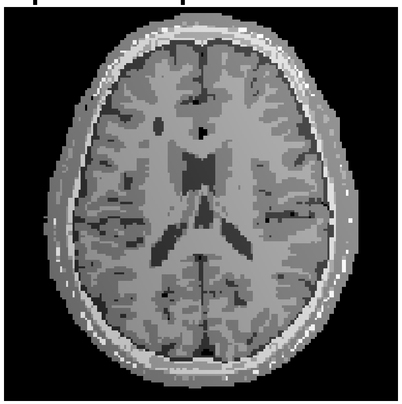

Example of quantitative MRI parameters (contains coil-sensitivity error $\hat{\rho} = \rho * C$)

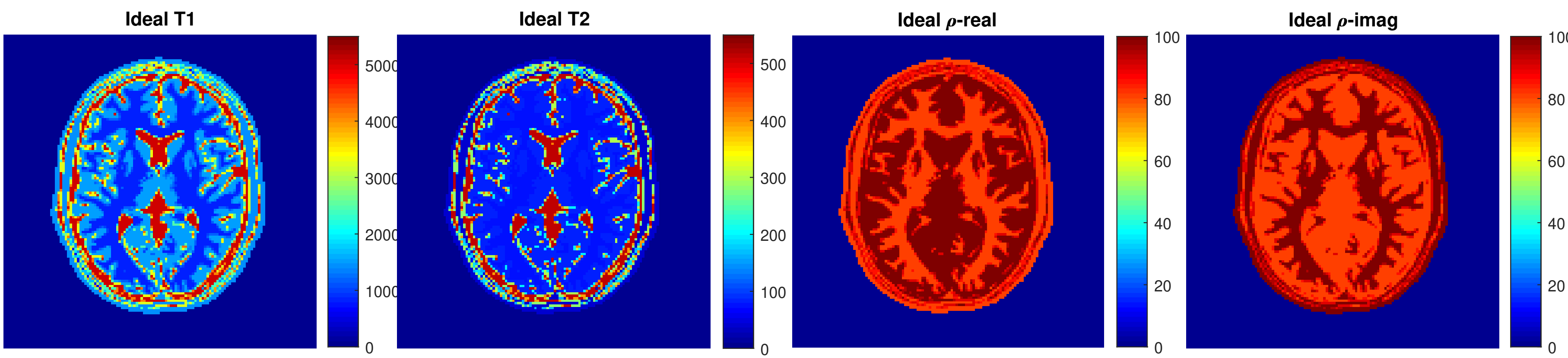

Qualitative MRI v.s. Quantitative MRI

Qualitative MRI

- inverting under-sampled Fourier data, mature techniques
- visualizing amplitude of magnetization for diagnosis
- T_1, T_2 or ρ weighted images by adjusting B_0, B_1
- reconstruction can be done apart from the physics behind

Quantitative MRI

- techniques still in experimental stage
- precisely measure the magnetic and tissue parameters e.g. $\theta = (T_1, T_2)^T$, and ρ
- imaging process is more time consuming
- physics (Bloch equations) explicitly entered into the reconstruction

Mathematical understanding of MRF-based methods

Magnetic resonance fingerprinting (MRF)

The working flow of the original MRF [a]:

- Create a dictionary Dic(C_{ad}) of magnetizations m: Solve Bloch equations for a variety of T_1, T_2. C_{ad} restricts (T_1, T_2) to their natural range.
- Reconstruct $X^* := (X^{(1)}, \ldots, X^{(L)})$ magnetization from the data:

$$X^{(l)} \in \operatorname*{argmin}_X \|P^{(l)}\mathcal{F}X - Y^{(l)}\|_2^2, \quad l = 1, \ldots, L.$$

  Match the reconstructed magnetization to a dictionary element:

$$m^* \in \operatorname*{argmin}_{m_{x,y} \in \text{Dic}(C_{ad})} S(m_{x,y}, X^*) \text{ with } X^* = (X^{(1)}, \ldots, X^{(L)}).$$

- Use look-up table to match (T_1, T_2) to m^*.

X^* might be non-unique and not optimal for under-sampled data!

[a] D. Ma et al. Magnetic resonance fingerprinting, Nature, **495**(187) (2013)

Other dictionary-based methods

The BLIP algorithm [a] applies projected gradient descent (also called projected Landweber iteration) to approximate the following optimization problem:

$$\min_{X} \quad \|P\mathcal{F}X - Y\|^2, \qquad \text{(BLIP)}$$
$$\text{subject to } X \in \mathbb{R}^+\mathrm{Dic}(C_{ad}).$$

- BLIP gives better reconstruction of the magnetization in MRF.
- From a geometric point of view, $\mathrm{Dic}(C_{ad})$ is a high dimensional manifold.
- The Bloch manifold is nonconvex with respect to $\theta = (T_1, T_2)^\top$, and the projection is ill-posed.
- Fineness of dictionary matters to the accuracy.

[a] M. Davies et al. A compressive sensing framework for magnetic resonance fingerprinting, SIAM J. Imag. Sciences, **7**(4) (2014)

Other dictionary-based methods

The FLOR algorithm[a] uses a low rank penalty for the representation of the magnetization in the dictionary:

$$\min_{X} \quad \|P\mathcal{F}X - Y\|^2 + \lambda \text{Rank}(X), \qquad \text{(FLOR)}$$

$$\text{subject to } X \in \mathbb{R}^+ \text{Dic}(C_{ad}).$$

- X is a vector spanned by only a few elements from Dic(C_{ad}).
- FLOR further optimizes the reconstructing and matching steps in MRF.
- Produces better results than BLIP in radial sub-sampling.
- Algorithm does not work well in Cartesian cases.
- Fineness of dictionary still matters.

[a] G. Mazor, L. Weizman, A. Tal, Y.C. Eldar. Low-rank magnetic resonance fingerprinting, Medical Physics, **45**(9), 2018

qMRI interpreted as coupled inverse problems

Dictionary based methods mostly approach qMRI problem from the following aspect: Solving two coupled (nonlinear) operator equations

$$PF(\rho m) = g,$$

and

$$\mathcal{B}(\theta) = m.$$

We have the following type of stability estimate[a]:

Theorem

Let $m, m^\delta \in$ Dic(C_{ad}), if $\|m - m^\delta\| \leq \delta$ for some positive $\delta > 0$, then there exist constant C

$$\|\theta - \theta^\delta\| \leq C\delta.$$

[a] G. Dong, M. Hintermüller, K. Papafitsoros. Quantitative magnetic resonance imaging: From fingerprinting to integrated physics-based models, SIAM J. Imag. Sciences, Vol. 12, No. 2, pp. 927–971, 2019.

Integrated physics-based method for qMRI

Integrated physics-based method for qMRI

- Integrate the two inverse problems into a single non-linear operator equation[a]:

$$Q(\rho, \theta) = g,$$

where

$$Q(\rho,\theta) := P\mathcal{F}(\rho T_{x,y} m(\theta)) \text{ and } [\rho(\mathbf{r}); \theta(\mathbf{r})] \in \mathcal{C}_{ad} := [\mathbb{R}^+; C_{ad}] \text{ for all } \mathbf{r} \in \Omega.$$

- Time continuous function $m(\theta)$ practically replaced by discrete dynamics $M(\theta)$ e.g. Inversion Recovery balanced Steady-State Free Precession.

- Some important properties are proven:
  - $M : [L^\infty(\Omega)]^2 \to [L^2(\Omega)]^3$ is Fréchet differentiable.
  - $M(C_{ad})$ is a non-convex set.
  - $Q : [L^\infty(\Omega)]^3 \to [L^2(K)]^3$ is Fréchet differentiable.

[a] G. Dong, M. Hintermüller, K. Papafitsoros. Quantitative magnetic resonance imaging: From fingerprinting to integrated physics-based models, SIAM J. Imag. Sciences, Vol. 12, No. 2, pp. 927–971, 2019.

Time discrete Bloch dynamics

In practice, discrete dynamic sequences $M = (M_l)_{l=1}^L$ (e.g. Inversion Recovery balanced Steady-State Free Precession flip angle sequence patterns)

$$\begin{cases} M_l &= E_1(TR_l, \theta) R_{\phi_l} R_x(\alpha_l) R_{\phi_l}^\top M_{l-1} + E_2(TR_l, \theta) M_e, \\ M_e &= (0,0,1)^\top, \\ M_0 &= -M_e = (0,0,-1)^\top. \end{cases}$$

where

$$E_1(TR_l, \theta) = \begin{pmatrix} e^{-\frac{TR_l}{T_2}} & 0 & 0 \\ 0 & e^{-\frac{TR_l}{T_2}} & 0 \\ 0 & 0 & e^{-\frac{TR_l}{T_1}} \end{pmatrix}, \qquad E_2(TR_l, \theta) = \left(1 - e^{-\frac{TR_l}{T_1}}\right)$$

$$R_{\phi_\ell} = \begin{pmatrix} \cos(\phi_\ell) & \sin(\phi_\ell) & 0 \\ -\sin(\phi_\ell) & \cos(\phi_\ell) & 0 \\ 0 & 0 & 1 \end{pmatrix} \text{ and } R_x(\alpha_\ell) = \begin{pmatrix} 1 & 0 & 0 \\ 0 & \cos(\alpha_\ell) & \sin(\alpha_\ell) \\ 0 & -\sin(\alpha_\ell) & \cos(\alpha_\ell) \end{pmatrix}.$$

M_l has a closed form:

$$M_l = \left(\prod_{k=1}^{l} E_1(TR_k, \theta) R(\alpha_k)\right) M_0 + E_2(TR_l, \theta) M_e + \sum_{k=1}^{l-1} \left(E_2(TR_k, \theta) \prod_{j=k+1}^{l} E_1(TR_j, \theta) R(\alpha_j)\right) M_e.$$

Gauss-Newton iteration

- Denote $u = (T_1, T_2, \rho)^\top$. Consider first order Taylor expansion:

$$Q(u_{n+1}) \simeq Q(u_n) + Q'(u_n)\,(u_{n+1} - u_n) = g,$$

suggests a projected Gauss-Newton iteration:

$$\begin{aligned}
g_n &= g - Q(u_n) + Q'(u_n)u_n, \\
v_{n+1} &= (Q')^\dagger(u_n)g_n := \left((Q'(u_n))^\top Q'(u_n)\right)^{-1}(Q'(u_n))^\top g_n, \\
u_{n+1} &= P_{\tilde{\mathcal{C}}_{ad}} v_{n+1}.
\end{aligned}$$

$$\text{where} \quad (P_{\tilde{\mathcal{C}}_{ad}} v)_p(r) = \begin{cases} \underline{C}_p & \text{for } v_p(r) \le \underline{C}_p \\ v_p(r) & \text{for } \underline{C}_p < v_p(r) < \overline{C}_p \\ \overline{C}_p & \text{for } \overline{C}_p \le v_p(r) \end{cases}$$

Converge superlinearly for proper initial values, but sensitive to noise.

A Levenberg-Marquardt method

- An estimation for $u,\ h \in [L^\infty(\Omega)]^3$, and $Q : [L^\infty(\Omega)]^3 \to \left([L^2(K)]^2\right)^L$:

$$\|Q(u+h) - Q(u) - Q'(u)h\|_{([L^2(K)]^2)^L} = o\left(\|h\|_{[L^2(\Omega)]^3}\right).$$

- L-M is a kind of regularization for the case of noisy and under-sampled data.

Key steps of the algorithm (Note now in Hilbert space ($[L^2(\Omega)]^3$)):

- Initialization: using BLIP algorithm with a coarse dictionary.
- A projected Levenberg-Marquardt iteration:

$$\begin{aligned} \tilde{g}_n^\delta &= g^\delta - Q(u_n) \\ h_n^\delta &= \underset{h}{\operatorname{argmin}} \|Q'(u_n)h - \tilde{g}_n^\delta\|^2_{([L^2(K)]^2)^L} + \lambda_n \|h\|^2_{[L^2(\Omega)]^3} \\ u_{n+1} &= P_{\tilde{\mathcal{C}}_{ad}}(u_n + h_n^\delta) \end{aligned}$$

with updated parameter $\lambda_n = \max\{\lambda_0 \beta^n, \mu_n\}$, where $\beta \in (0,1)$, and $\mu_n \geq 0$.

Numerical results on qMRI–Cartesian subsampling case

Solution of BLIP algorithm

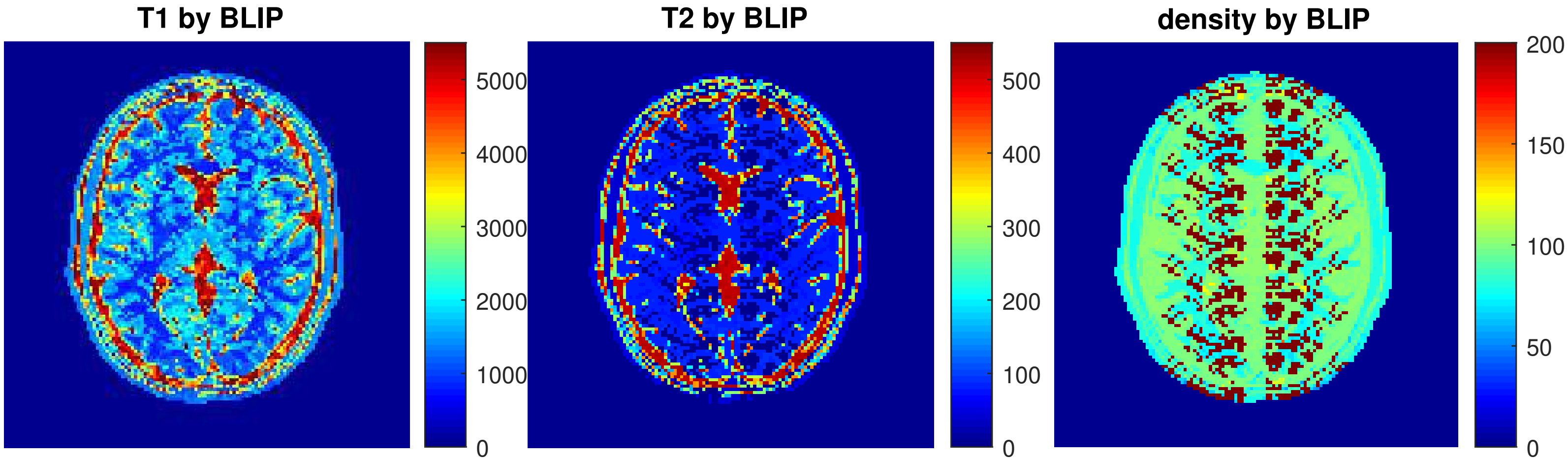

Solution of proposed method

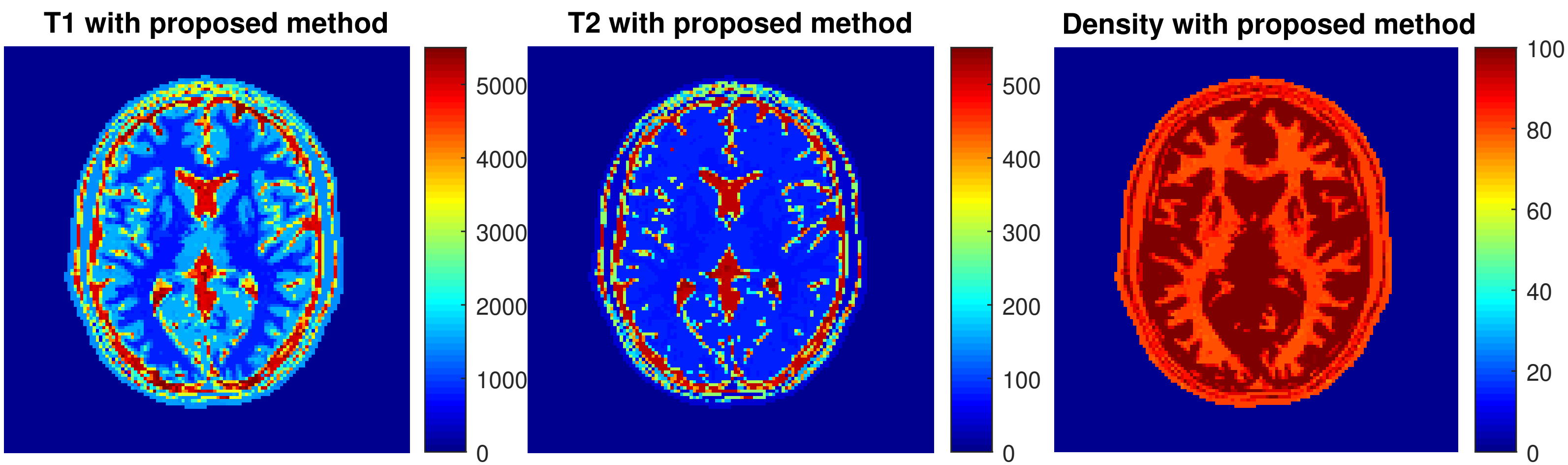

Numerical results on qMRI–Cartesian subsampling case

Relative error map from BLIP algorithm

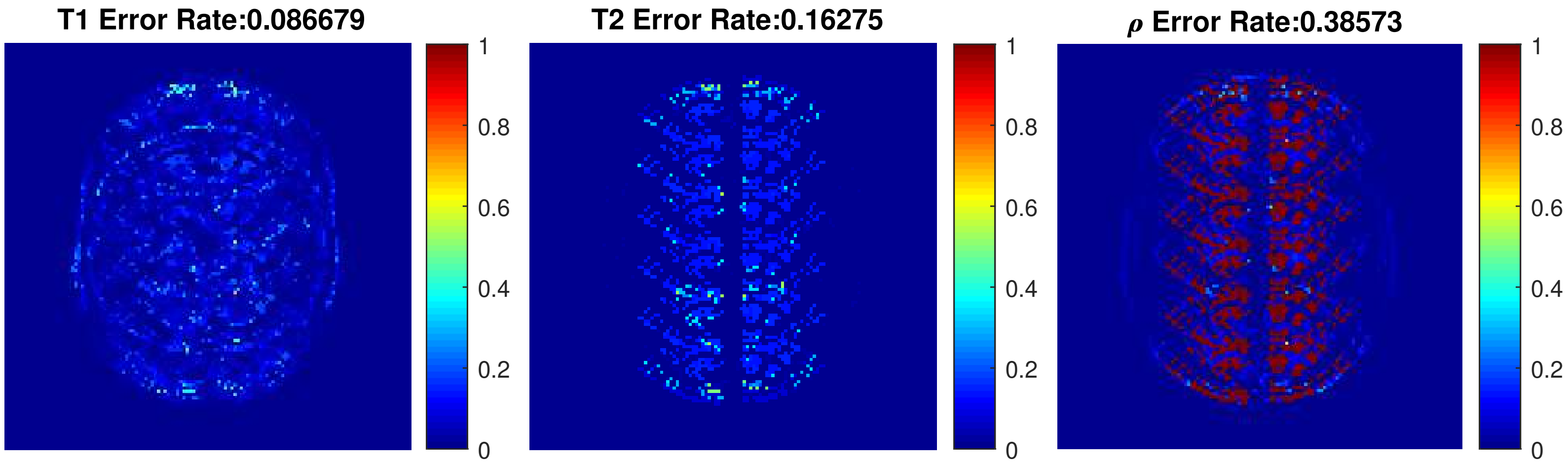

Relative error map from proposed method

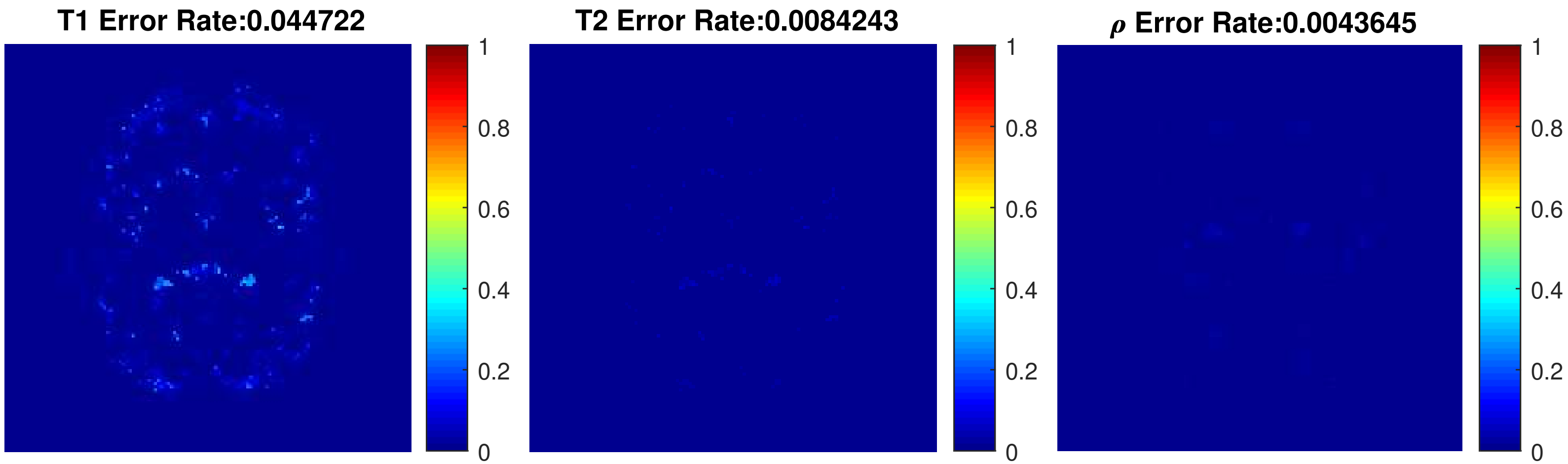

Numerical results on qMRI–Radial subsampling case

Solution of FLOR algorithm

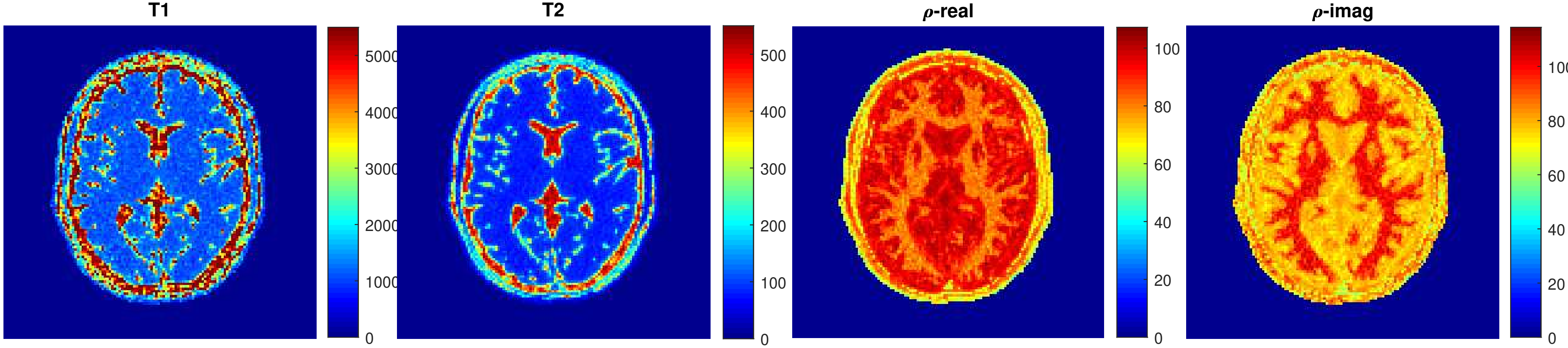

Solution of proposed method

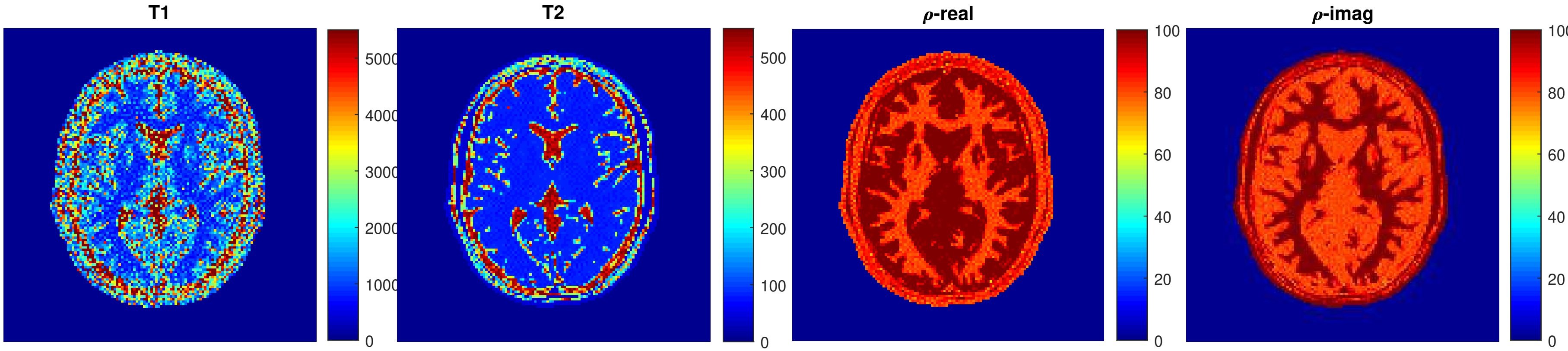

Numerical results on qMRI–Radial subsampling case

Relative error map from FLOR algorithm

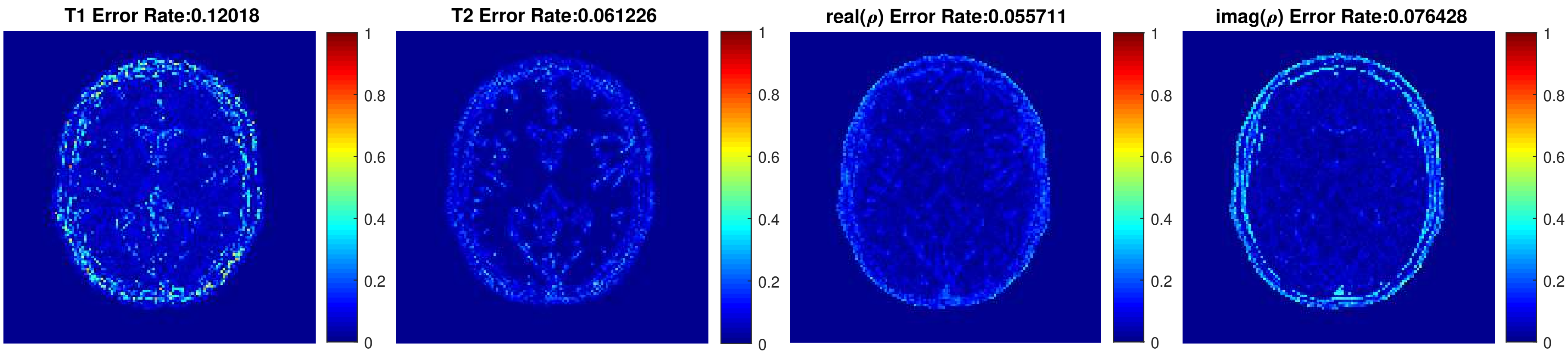

Relative error map from proposed method

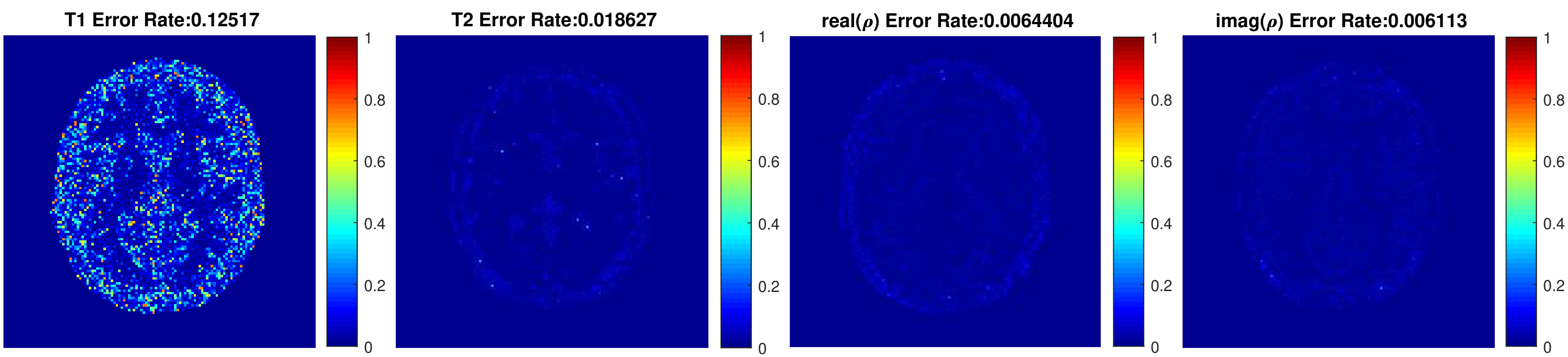

Using learning-informed physical models

Optimization with (learning-informed) physics-constraints [1]

- A general physics-based inverse (imaging) problem:

$$Ay = g, \quad \text{given } g \in H$$
$$\text{where } e(y,u) = 0 \text{ for } (y,u) \in Y \times U \text{ and } u \in \mathcal{C}_{ad}$$

Let $y = \Pi(u)$ be an explicit representation of $e(y,u) = 0$ (e.g., solution map of Bloch equations, $u = \theta = (T_1, T_2, \rho)$).

- We study the following generic problem:

$$\begin{aligned} \underset{(y,u)\in(Y\times U)}{\text{minimize}} \quad & \frac{1}{2}\|Ay - g^\delta\|_H^2 + \frac{\alpha}{2}\|u\|_U^2, \\ \text{subject to} \quad & e(y,u) = 0, \\ & u \in \mathcal{C}_{ad}. \end{aligned}$$

[1] G. Dong, M. Hintermüller, K. Papafitsoros. Optimization with learning-informed differential equation constraints and its applications, ESAIM: Control, Optimisation and Calculus of Variations, 2021.

Optimization with (learning-informed) physics-constraints [1]

- A general physics-based inverse (imaging) problem:

$$Ay = g, \quad \text{given } \; g \in H$$
$$\text{where } \; e(y,u) = 0 \; \text{ for } \; (y,u) \in Y \times U \; \text{ and } \; u \in \mathcal{C}_{ad}$$

Let $y = \Pi(u)$ be an explicit representation of $e(y,u) = 0$ (e.g., solution map of Bloch equations, $u = \theta = (T_1, T_2, \rho)$).

- We study the following generic problem:

$$\underset{u}{\text{minimize}} \quad \frac{1}{2}\|A\Pi(u) - g^\delta\|_H^2 + \frac{\alpha}{2}\|u\|_U^2 =: \mathcal{J}(u),$$
$$\text{subject to} \quad u \in \mathcal{C}_{ad}.$$

[1] G. Dong, M. Hintermüller, K. Papafitsoros. Optimization with learning-informed differential equation constraints and its applications, ESAIM: Control, Optimisation and Calculus of Variations, 2021.

Optimization with (learning-informed) physics-constraints [1]

- A general physics-based inverse (imaging) problem:

$$Ay = g, \quad \text{given } g \in H$$
$$\text{where } e(y,u) = 0 \text{ for } (y,u) \in Y \times U \text{ and } u \in \mathcal{C}_{ad}$$

Let $y = \Pi(u)$ be an explicit representation of $e(y,u) = 0$ (e.g., solution map of Bloch equations, $u = \theta = (T_1, T_2, \rho)$).

- We study the following generic problem:

$$\underset{u}{\text{minimize}} \quad \frac{1}{2}\|A\Pi_{\mathcal{N}}(u) - g\|_H^2 + \frac{\alpha}{2}\|u\|_U^2 =: \mathcal{J}_{\mathcal{N}}(u),$$
$$\text{subject to} \quad u \in \mathcal{C}_{ad}.$$

[1] G. Dong, M. Hintermüller, K. Papafitsoros. Optimization with learning-informed differential equation constraints and its applications, ESAIM: Control, Optimisation and Calculus of Variations, 2021.

Artificial Neural Network

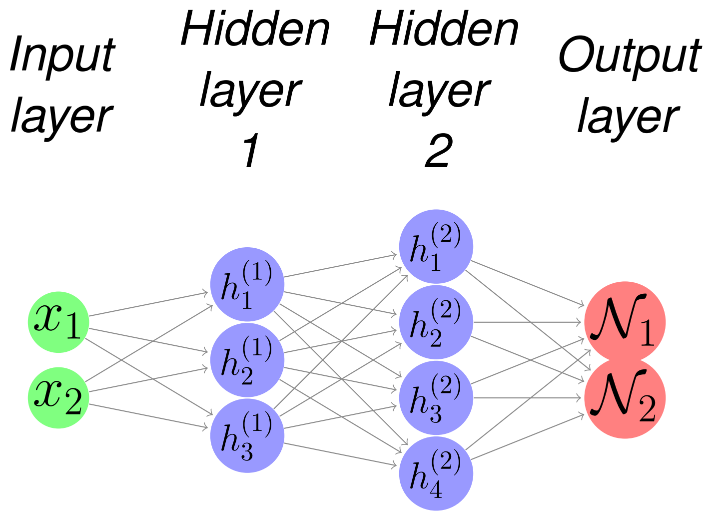

A fully connected multi-layer feedforward ANN.

From one layer to the next: connected by affine mapping and activation function

$$\mathbf{h} = \sigma(\mathbf{z}) = \sigma(W\mathbf{x} + \mathbf{b}).$$

Universal approximation theorem for ANNs[2]

ANNs have been very successful approximators for functions $f : \Omega \to \mathbb{R}^n$, defined on bounded $\Omega \subset \mathbb{R}^m$.

Theorem (function value approximation)

A standard multi-layer feedforward network with a continuous activation function can uniformly approximate any continuous function to any degree of accuracy if and only if its activation function is not a polynomial.

Theorem (derivative approximation)

There exists a neural network which can approximate both the function value and the derivatives of f uniformly to any degree of accuracy if the activation function is continuously differentiable and is not a polynomial.

[2] Pinkus, Approximation theory of the MLP model in neural networks. Acta Numerica, 1999.

Activation functions of ANNs

Examples of smooth activation functions:

- *Sigmoid: e.g., tansig* ($\sigma(z) = \frac{e^z - e^{-z}}{e^z + e^{-z}}$), *logsig* ($\sigma(z) = \frac{1}{1+e^{-z}}$)), *arctan* ($\sigma(z) = \arctan(z)$), *etc.*
- *Probability functions: e.g., softmax* ($\sigma_i(z) = \frac{e^{-z_i}}{\sum_j e^{-z_j}}$)

Examples of nonsmooth activation functions:

- *ReLU: Rectified Linear Unit* ($\sigma(z) = \max(0, z)$)

Important: *Choosing smooth vs. nonsmooth activation functions should respect prior information on to be approximated object and has numerous implications in optimization.*

Remark on neural network approximation

NNs approximate an objective f in different settings	Examples
1. $f : \Omega \subset \mathbb{R}^m \to \mathbb{R}^n$, with finite m and n Universal approximation theorem	(Generalized) Regression
2. $f : \mathcal{K} \subset \mathcal{B}_1 \to \mathbb{R}^n$, where $\mathcal{B}_1$ is some Banach space Under-development (mostly convolutionary NNs)	(Image) Classification
3. $f : \Omega \subset \mathbb{R}^m \to \mathcal{B}_2$, where $\mathcal{B}_2$ is some Banach space Under-development (many different methods)	Solving (partial) differential equations
4. $f : \mathcal{K} \subset \mathcal{B}_1 \to \mathcal{B}_2$, $(\mathcal{B}_k)_{k=1}^2$ can be infinite dimensional Under-development (very few still)	Operator learning

Except for case 1, mathematical understanding of cases 2–4 still mostly in progress.

Main difficulty: Compactness condition problematic.

A diagram of the proposed general framework

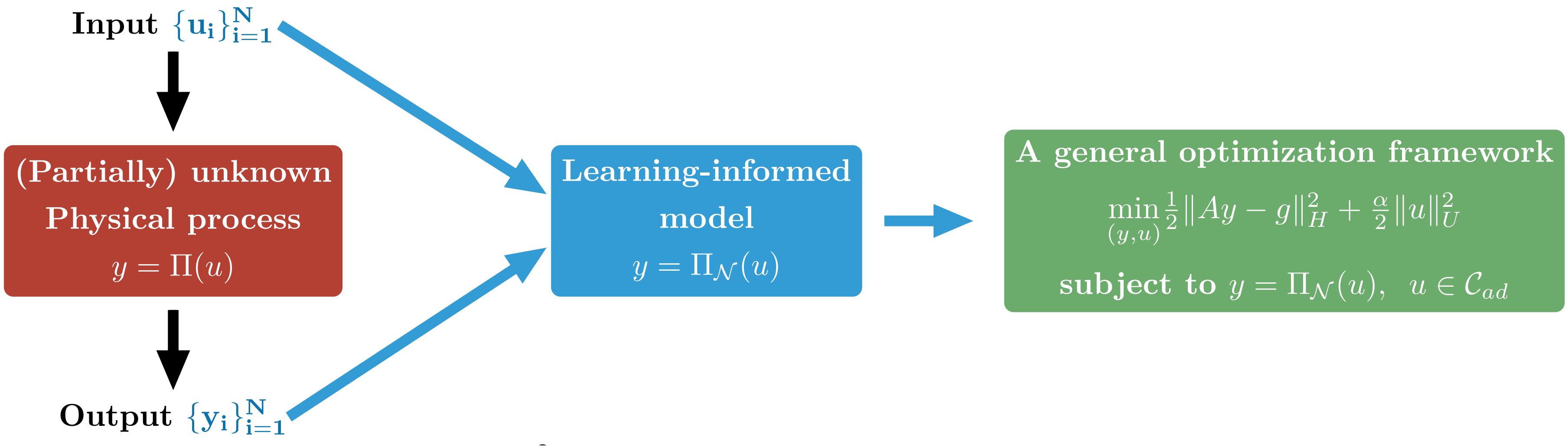

Fundamental questions:

- Conditions for well-posedness of learned physical model and universal approximation property of $\Pi_{\mathcal{N}} \sim \Pi$.
- Approximation properties of optimizers associated to learning-informed models vs. those related to original physics-based models.

Some analytical aspects

Denote $Q := A\Pi$ (or $A\Pi_{\mathcal{N}}$) the reduced operator.

Theorem

Suppose that Q is weakly-weakly sequentially closed, i.e., if $u_n \overset{U}{\rightharpoonup} u$ and $Q(u_n) \overset{H}{\rightharpoonup} \bar{g}$, then $\bar{g} = Q(u)$. Then the optimization problem admits a solution $\bar{u} \in U$.
In the special case when $\mathcal{C}_{ad}$ is a bounded set of a subspace $\hat{U}$ compactly embedded into U, then strong-weak sequential closedness of Q is sufficient to guarantee existence of a solution.

- *In many PDE models, regularity of the resp. solution helps the weak-weak sequential closedness condition of the control-to-state map to be satisfied.*
- *While in imaging applications (inverse problems, more generally) regularization usually plays a role similar to $\hat{U}$.*

Convergence under operator perturbations

Let $Q_n := A\Pi_{\mathcal{N}_n}$ be the reduced learning-informed operators.

Theorem

Let Q and Q_n for $n \in \mathbb{N}$ be weakly sequentially closed operators, and

$$\sup_{u\in\mathcal{C}_{ad}} \|Q(u) - Q_n(u)\|_H \leq \epsilon_n, \quad \textit{for} \quad \epsilon_n \downarrow 0.$$

Suppose $(u_n)_{n\in\mathbb{N}}$ is a sequence of minimizers associated to the optimization problems with reduced operator Q_n for all $n \in \mathbb{N}$.
Then, there is the strong convergence (up to a sub-sequence)

$$u_n \to \bar{u} \;\; \textit{in} \;\; U, \quad \textit{and} \quad Q_n(u_n) \to Q(\bar{u}) \;\; \textit{in} \;\; H, \quad \textit{as} \;\; n \to \infty,$$

where $\bar{u}$ is a minimizer of the original optimization problem.

Convergence rates

Denote L_0 and L_1 the Lipschitz constants associated to Q and Q', respectively, where Q' is the Fréchet derivative of Q, and $\eta_n := \|Q' - Q'_n\|_{\mathcal{L}(U,H)}$.

Theorem

Under smallness of L_0, L_1, the solutions u_n converge to $\bar{u}$ at the following rate

$$\|u_n - \bar{u}\|_U = \mathcal{O}\left(L_0\epsilon_n + \|Q(\bar{u}) - g\|_H \eta_n\right).$$

Theorem (when $\mathcal{J}'(\bar{u}) = 0$)

Suppose the Lipschitz constant L_1 satisfies

$$L_1 \|Q(\bar{u}) - g\|_H < \alpha.$$

If $\mathcal{J}'(\bar{u}) = 0$, then for sufficiently large $n \in \mathbb{N}$ we have the following error bound

$$\|u_n - \bar{u}\|_U = \mathcal{O}\left(\sqrt{\epsilon_n^2 + 2\|Q(\bar{u}) - g\|_H^2}\right).$$

Application to qMRI

qMRI as a „control problem"

qMRI fits the general optimization framework:

$$\underset{(y,u)}{\text{minimize}} \quad \frac{1}{2}\|P\mathcal{F}(y) - g^\delta\|_H^2 + \frac{\alpha}{2}\|u\|_U^2,$$

subject to

$$\frac{\partial y}{\partial t}(t) = y(t) \times \gamma B(t) - \left(\frac{y_1(t)}{T_2}, \frac{y_2(t)}{T_2}, \frac{y_3(t) - \rho m_e}{T_1}\right), \; t = t_1, \ldots, t_L,$$
$$y(0) = \rho m_0,$$
$$u \in \mathcal{C}_{ad}.$$

- The goal is to estimate the physical parameters $u = (\rho, T_1, T_2)$

qMRI as a „control problem”

qMRI fits the general optimization framework:

$$\underset{(y,u)}{\text{minimize}} \quad \frac{1}{2}\|P\mathcal{F}(y) - g^\delta\|_H^2 + \frac{\alpha}{2}\|u\|_U^2,$$

subject to

$$\begin{aligned} y &= \mathcal{N}(u), \\ u &\in \mathcal{C}_{ad}. \end{aligned}$$

- The goal is to estimate the physical parameters $u = (\rho, T_1, T_2)$
- ANNs $\mathcal{N}$ approximate the parameter-to-solution map (Nemytskii type):

$$(\rho, T_1, T_2) \mapsto (y_{t_1}, \dots, y_{t_L})$$

Universal approximation of learning-informed Bloch operator

Both Π and $\Pi_{\mathcal{N}} = \mathcal{N}$ are operators of Nemytskii type in the qMRI case.

Theorem

The operator $\Pi : \mathcal{C}_{ad} \subset [L^\infty_\epsilon(\Omega)^+]^3 \to [(L^\infty(\Omega))^3]^L$ is Lipschitz continuous, and Fréchet differentiable with locally Lipschitz derivative.

Theorem

Let $u = (T_1, T_2, \rho)^\top \in \mathcal{C}_{ad}$. Then for arbitrary small $\epsilon > 0$ and $\epsilon_1 > 0$, there always exist neural network approximations so that

$$\|\Pi_{\mathcal{N}}(u) - \Pi(u)\|_{[L^\infty(\Omega)^3]^L} \le \epsilon,$$

and

$$\|\Pi'_{\mathcal{N}}(u) - \Pi'(u)\|_{\mathcal{L}([L^2(\Omega)]^3,[L^\infty(\Omega)^3]^L)} \le \epsilon_1,$$

are satisfied.

A sequential quadratic programming (SQP) algorithm

Define

$$\mathcal{J}_{\mathcal{N}}(u) := \frac{1}{2}\|P\mathcal{F}(\mathcal{N}(u)) - g^{\delta}\|_H^2 + \frac{\alpha}{2}\|u\|_U^2.$$

The derivative $\mathcal{J}'_{\mathcal{N}}(u)$ has an explicit form

$$(\rho(\mathcal{N}'(T_1,T_2))^*, \mathcal{N}(T_1,T_2))^\top \mathcal{F}^*(\mathcal{F}(\rho\mathcal{N}(T_1,T_2)) - g) + \alpha(\mathsf{Id} - \Delta)(T_1,T_2,\rho)^\top.$$

Every QP-step solves

$$\begin{aligned} \text{minimize} \quad & \langle \mathcal{J}'_{\mathcal{N}}(u_k), h\rangle_{U^*,U} + \frac{1}{2}\langle H_k(u_k)h, h\rangle_{U^*,U} \quad \text{over } h \in U \\ \text{s.t.} \quad & u_k + h \in \mathcal{C}_{ad}, \end{aligned}$$

where $H_k(u_k)$ is a pos.-def. approx. of the Hessian of $\mathcal{J}_{\mathcal{N}}$ at $u_k \in \mathcal{C}_{ad}$:

$$(\rho(\mathcal{N}'(T_1,T_2))^*, \mathcal{N}(T_1,T_2))^\top \mathcal{F}^*\mathcal{F}(\rho(\mathcal{N}'(T_1,T_2)), \mathcal{N}(T_1,T_2)) + \alpha(\mathsf{Id} - \Delta).$$

Numerical results on synthetic data

Solutions using the proposed learning-informed method

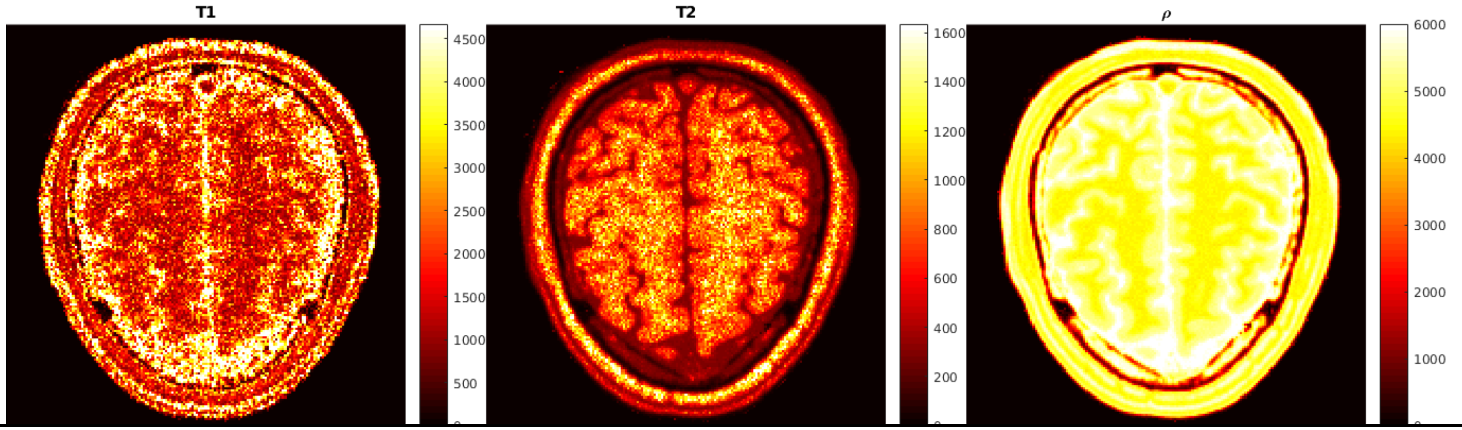

Solutions using previous physics-integrated method

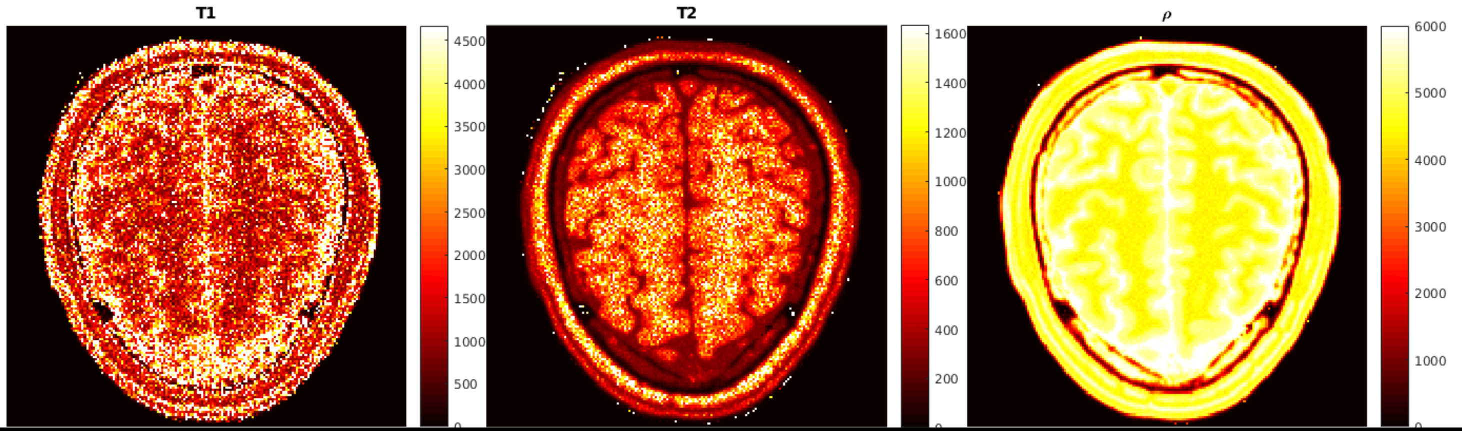

Numerical results on synthetic data

Error map from the proposed learning-informed method

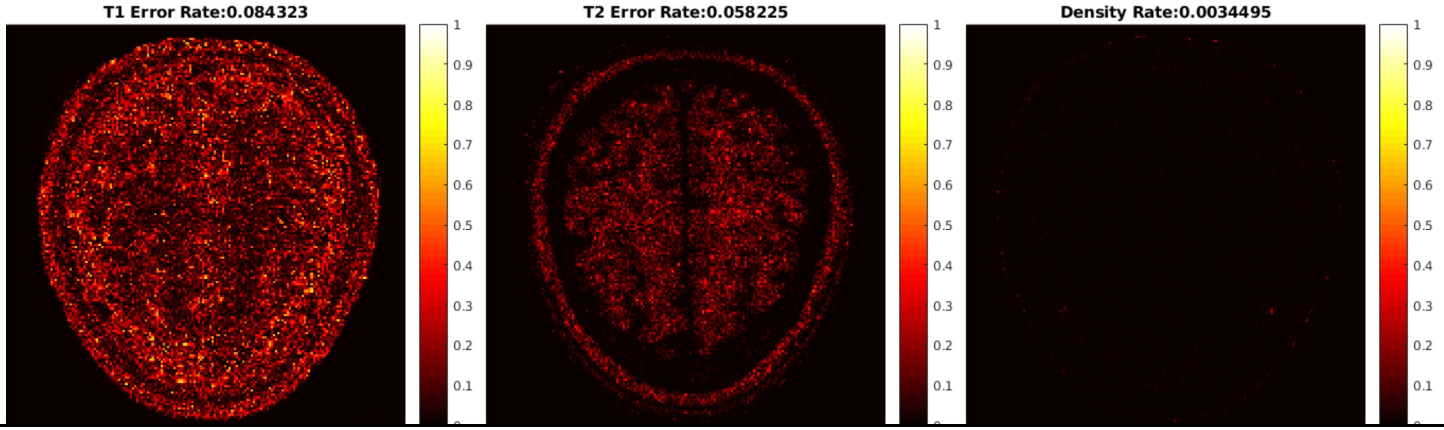

Error map from previous physics-integrated method

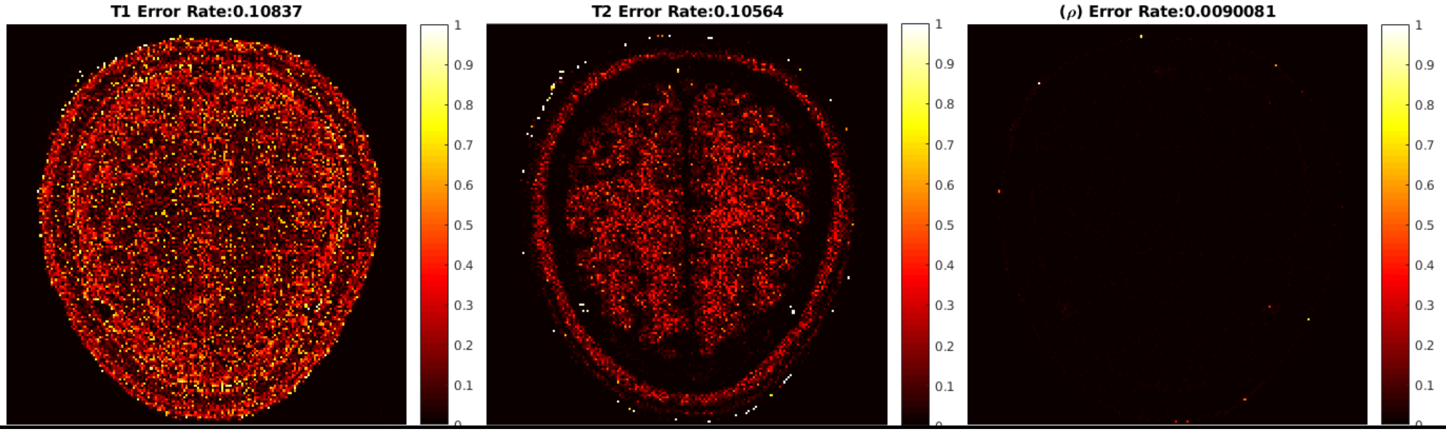

Summary

- Mathematical understanding of MRF type methods for qMRI.
- Integrated physics-based model for qMRI.
- Learning-informed model for explicit representations of physical operators.
- Mathematical analysis for the proposed methods and robust numerical algorithms.

Thank you for your attention!